THE ASTROPHYSICAL JOURNAL, 551:103–110, 2001 April 10

CONTINUUM VARIABILITY OF ACTIVE GALACTIC NUCLEI IN THE OPTICAL–ULTRAVIOLET RANGE

DARIO TRÈVESE[1]
Dipartimento di Fisica, Università di Roma "La Sapienza," Piazzale A. Moro 2, I-00185 Roma, Italy; dario.trevese@roma1.infn.it
RICHARD G. KRON[1]
Fermi National Laboratory, MS 127, Box 500, Batavia, IL 60510; rich@oddjob.uchicago.edu
AND
ALESSANDRO BUNONE
Dipartimento di Fisica, Università di Roma "La Sapienza," Piazzale A. Moro 2, I-00185 Roma, Italy
Received 2000 January 20; accepted 2000 December 15

ABSTRACT

The variability of the continuum spectral energy distribution has been analyzed for a complete magnitude-limited sample of quasars in Selected Area 57, observed at two epochs in the photographic U, B_J, F, and N bands with the Mayall 4 m telescope at Kitt Peak National Observatory. Changes $\delta\alpha$ of the spectral slope α appear correlated with brightness variations $\delta \log f_\nu$, indicating an average hardening of the spectrum in the bright phases. This confirms that the correlation of variability with redshift, found in a single observing band, is due to intrinsic spectral changes. The average observed $\delta\alpha$–$\delta \log f_\nu$ relation is consistent with the spectral change due to temperature variation of a blackbody of about 2.5×10^4 K.

Subject headings: galaxies: active — galaxies: fundamental parameters — galaxies: Seyfert — quasars: general — techniques: photometric

On-line material: machine-readable table

1. INTRODUCTION

Variability provides a powerful tool for constraining the physics of active galactic nuclei (AGNs). The original models based on a central black hole surrounded by an accretion disk (Rees 1984) were based on the constraints on the source size and energy density provided by the early single-band variability studies. Single-epoch multiwavelength observations, covering simultaneously the range from radio to gamma-ray frequencies, are of crucial importance in suggesting the physical mechanisms responsible for the emission. However, in general they cannot sufficiently constrain the large number of parameters involved in models. So far multiwavelength monitoring, with adequate time sampling and duration, has been possible for a small number of low-redshift objects, thanks to large international collaborations (see the review of Ulrich, Maraschi, & Urry 1997 and references therein). These observations provided further clues to and constraints on the radiation processes and reprocessing mechanisms, since changes of the spectral energy distribution (SED) associated with flux variations can be interpreted in terms of an interplay of emission components of different spectral shape and variability properties. Various classes of AGNs show different variability properties. Blazars show strong (greater than 1 mag) variations of the observed fluxes on timescales from days to months from radio to gamma frequencies, while in the optical–UV Seyfert 1 and normal quasars (QSOs) show smaller (less than 0.5 mag) variability on timescales greater than a few months, although greater than 1 mag variations on timescales of days have been detected in X-rays in some Seyfert galaxies (Mushotzki, Done, & Pounds 1993 and references therein; in the following we ignore the traditional distinction at $M_B = -23$ between Seyfert 1 galaxies and QSOs). The result of multifrequency monitoring indicates that the optical–UV continuum of AGNs hardens during the bright phases (Cutri et al. 1985; Edelson, Krolik, & Pike 1990; Kinney et al. 1991; Paltani & Courvoisier 1994) in the near-infrared–optical–UV range, while little or no correlation is thought to be present in BL Lac objects (Edelson 1992; see, however, Massaro et al. 1996).

Optical observations at faint magnitudes ($B \approx 20$–23 mag) enable magnitude-limited statistical samples to be constructed (mostly of radio-quiet objects) in a single field of a large telescope, and repeated broadband imaging provides light curves for each AGN in the sample (Hawkins 1983; Koo & Kron 1988; Trèvese et al. 1989, hereafter T89; Trèvese et al. 1994, hereafter T94; Cristiani, Vio, & Andreani 1990; Hawkins & Véron 1993, 1996; Bershady, Trèvese, & Kron 1998, hereafter BTK98), allowing the ensemble variability properties of the sample to be assessed.

Studies of this kind are complicated by the fact that in all magnitude-limited samples the luminosity is strongly correlated with redshift (L-z correlation), since the majority of objects lie close to the limiting flux. This makes it difficult to isolate the intrinsic variability-luminosity (v-L) and variability-redshift (v-z) correlations.

Since early studies, the relation between absolute optical luminosity and optical variability has been addressed by several authors (Angione & Smith 1972; Uomoto, Wills, & Wills 1976; Pica & Smith 1983), with the aim of discovering whether QSOs are made up of multiple sources or single coherent sources. In the former case, a decrease of variability amplitude with luminosity is expected. In recent years, consensus has progressively grown that brighter QSOs are less variable on average (T94; Hook et al. 1994; Cristiani et al. 1996; see Giveon et al. 1999 for a recent summary). This would seem to support a model in which the active nucleus is powered by a series of supernova explosions (Aretxaga & Terlevich 1994; Aretxaga, Cid Fernandes, & Terlevich 1997), though this model can fail to reproduce the variability amplitude in the case of most luminous QSOs, according

[1] Visiting Astronomer, Kitt Peak National Observatory, National Optical Astronomy Observatories, which are operated by the Association of Universities for Research in Astronomy, Inc., under cooperative agreement with the National Science Foundation.

to Hawkins (2000). A similar negative correlation of X-ray variability with the 1–10 keV luminosity was found in Seyfert galaxies and QSOs and interpreted in terms of a large number of incoherent flaring subunits by Green, McHardy, & Letho (1993). On the contrary, a positive v-L correlation was found by Edelson (1992) for the blazar population.

Concerning the L-z correlation, the situation is further complicated by the fact that the different variability indicators, used by different authors, are affected in different ways by the v-L and L-z correlations and by spurious redshift dependence due to the combination of time dilation, intrinsic variability timescales, and total duration of the observational campaign. This led Giallongo, Trèvese, & Vagnetti (1991, hereafter GTV91) to introduce a variability indicator based on the rest-frame structure function. Adopting this indicator, they found a positive correlation of variability with redshift, taking properly into account the effect of the v-L and L-z correlations. This result has been subsequently confirmed by the analysis of the QSO structure function in bins of luminosity and redshift, performed by Cristiani et al. (1996) using all the statistical samples available at that time.

GTV91 suggested that the v-z correlation can be explained by a hardening of the spectrum in the bright phases (and vice versa), coupled with the increase of the rest-frame frequency with redshift, for a fixed observing band.

Di Clemente et al. (1996), on the basis of the analysis of various QSO samples, have shown that indeed, on average, variability increases with the rest-frame frequency. This provides an indirect statistical argument for a slope change of the quasar SED associated with luminosity variability. Moreover, the increase of variability with rest-frame frequency is quantitatively consistent with the v-z correlation.

However, a direct statistical quantification of the change of spectral slope associated with luminosity variation is still missing. Moreover, even though variability has historically played a key role in constraining models of the QSO central engine, the physics of variability is still largely unknown. In fact, quite diverse variability mechanisms have been proposed, including supernovae explosions (Aretxaga & Terlevich 1994), instabilities in the accretion disk (Kawaguchi et al. 1998), and gravitational lensing due to intervening matter (Hawkins & Véron 1993; Hawkins 2000). Discriminating between these different models on the sole basis of single-band correlation functions and v-L and v-z correlations is a very difficult task.

In the present paper we analyze UB_JFN photometry of the faint QSO sample of SA 57 to look for direct evidence of an average spectral hardening for increasing flux. A statistical quantification of the spectral slope changes as a function of luminosity variations provides a new constraint for models of the variability mechanism. We also discuss the consistency of the SED variations with the v-z correlation and with temperature changes of an emitting blackbody.

This paper is organized as follows: data and reduction procedures are described in § 2, the statistical analysis of SED changes and their relation with flux variations are described in § 3, and a concluding discussion is presented in § 4.

2. THE AGN SAMPLE AND THE SPECTRAL ENERGY DISTRIBUTIONS

Statistical studies of variability require a QSO sample based on clearly known selection criteria, whose effects are clearly understood and quantifiable. Among the existing QSO samples, the magnitude-limited sample of faint QSOs of SA 57 (Kron & Chiu 1981; Koo, Kron, & Cudworth 1986, hereafter KKC86) is probably the most studied. This field has been repeatedly observed since 1974 with the Mayall 4 m telescope at Kitt Peak National Observatory in the photographic U, B_J, F, and N bands. Different techniques, such as colors, lack of proper motion, and variability, have been applied to search for AGNs down to $B_J = 23$ and to estimate the completeness of the sample. Spectroscopic confirmation of almost all of the QSO candidates has been obtained (Kron & Chiu 1981; KKC86; Koo & Kron 1988; T89; Majewski et al. 1991; T94), with the exception of the faint part of the sample of extended sources of BTK98. This allows us for the first time to perform a statistical analysis of the variability of the spectral energy distribution of QSOs. Single-band variability studies (T89; T94; BTK98) of the AGN sample where based on the entire collection of J (or B_J) plates. However, as discussed in the next section, the most reliable analysis of SED variability is obtained considering only "simultaneous" U, B_J, F, and N observations. For this reason we selected the two sets of plates taken in 1984 April and in 1985 April. The list of the plates is given in Table 1, which contains plate identification, the date, and the photometric band. The effective bandwidths of the U, B_J, F, and N bands are 570, 1250, 1150, and 1720 Å, respectively, and the effective wavelengths are 3540, 4460, 5980, and 7830 Å, respectively.

Photometric methods and signal-to-noise ratio optimization are described in T89, T94, and BTK98. The AGN sample consists of 40 spectroscopically confirmed objects. Table 2 gives the photometry on each of the nine plates considered in the present analysis.

Of these 40 objects, 35 are the QSOs discussed in T94, while another five objects are the spectroscopically confirmed AGNs selected by BTK98 as variable objects with extended images. The limiting magnitude of the sample is $m_2 < 23.5$ mag, where m_2 is the B_J magnitude evaluated in a fixed aperture of radius 0.″5 (but see BTK98 for faint extended objects). The cumulative redshift distribution has 25%, 50%, and 75% of the objects below $z = 0.75$, 1.16, and 1.80, respectively.

Figure 1 shows the Hubble diagram of the sample. Figure 2 shows a comparison of the U, B_J, and F fluxes at one epoch (1984 April), normalized at $\lambda = 2000$ Å, as a function of the rest-frame frequency. Most objects have similar spectral slopes, with five main exceptions, which are objects with a much steeper spectrum. Two of them are low redshift and two are the highest redshift objects. The former two, N_{ser}

TABLE 1

PLATE JOURNAL

MPF	UT Date	Band
3919.....	1984 Apr 05	B_J
3920.....	1984 Apr 05	U
3921.....	1984 Apr 05	B_J
3922.....	1984 Apr 05	F
3923.....	1984 Apr 05	N
3973.....	1985 Apr 25	N
3975.....	1985 Apr 26	F
3976.....	1985 Apr 25	U
3977.....	1985 Apr 25	B_J

TABLE 2

SUMMARY OF OBSERVATIONS

N_{694} (1)	N_{2540} (2)	N_{ser} (3)	KKC86 (4)	α_{1950} (5)	δ_{1950} (6)	m_4 (7)	z (8)	B_J(3919) (9)	U(3920) (10)	B_J(3921) (11)	F(3922) (12)	N(3923) (13)	N(3973) (14)	F(3975) (15)	U(3976) (16)	B_J(3977) (17)
4	11	100360	54	13 06 36.23	29 21 55.8	19.43	0.75	19.70	18.46	19.40	18.71	18.41	18.65	18.66	18.70	19.82
255.....	902	107624	28	13 05 53.15	29 35 15.9	19.59	1.74	19.40	18.37	19.34	18.74	18.63	18.67	18.90	18.45	19.42
389.....	1427	111610	22	13 05 48.99	29 41 10.6	19.81	3.02	19.07	19.72	19.33	18.14	18.14	17.97	18.14	19.57	19.04
613.....	2278	117750	19	13 05 45.60	29 50 46.7	19.87	1.18	19.81	18.83	19.80	19.05	19.10	19.03	19.17	18.95	19.68
563.....	2138	116713	10	13 05 26.41	29 49 01.7	20.14	0.99	19.62	18.86	19.62	19.03	19.31	19.23	19.12	18.91	19.51
109.....	412	103544	50	13 06 26.74	29 28 42.3	20.20	0.55	20.75	19.59	20.51	20.44	20.07	20.08	20.41	19.87	21.06
	51	100681	...	13 05 42.88	29 22 52.4	20.37	0.40	20.25	19.30	20.17	19.75	19.42	19.33	19.70	19.32	20.03
654.....	2410	118749	55	13 06 41.23	29 52 33.3	20.41	1.09	20.22	19.65	20.26	19.99	20.02	19.97	19.86	19.84	20.28
254.....	899	107567	37	13 06 09.20	29 35 09.7	20.60	1.81	20.83	20.20	20.82	20.68	20.35	20.34	20.85	20.24	20.95
160.....	606	105141	34	13 06 04.31	29 31 23.1	20.62	1.09	20.83	20.01	20.78	20.41	20.49	20.52	20.30	19.85	20.61
187.....	686	105767	...	13 05 15.05	29 32 25.0	20.73	0.71	20.79	20.62	20.77	20.00	19.32	19.38	20.11	20.64	20.78
172.....	641	105422	64	13 06 49.05	29 31 49.7	20.76	1.08	19.73	18.99	19.76	19.44	19.42	19.89	19.71	19.44	19.87
	1821	114264	...	13 05 40.52	29 45 07.1	20.77	0.29	20.66	20.92	20.72	19.01	18.41	18.23	19.19	20.62	20.43
335.....	1184	109980	25	13 05 50.30	29 38 42.1	20.78	1.55	20.71	19.87	20.72	20.60	20.38	20.29	20.69	20.07	20.74
30	88	101012	32	13 06 02.22	29 23 44.1	21.01	2.28	20.36	19.99	20.30	20.14	20.11	20.59	20.55	20.11	20.55
459.....	1772	113966	46	13 06 21.32	29 44 37.6	21.09	0.95	20.96	20.14	21.04	20.84	20.51	20.95	20.99	20.31	21.11
42	130	101339	44	13 06 17.75	29 24 33.3	21.15	0.00	21.05	20.50	21.01	20.76	20.53	20.62	20.91	20.58	21.17
240.....	856	107326	43	13 06 16.89	29 34 48.1	21.17	0.59	20.95	20.19	20.89	20.63	20.09	20.15	20.39	19.94	20.62
40	121	101304	11	13 05 27.05	29 24 30.0	21.21	2.27	20.98	20.56	20.98	20.93	21.60	21.78	21.24	21.11	21.27
371.....	1363	111178	...	13 07 23.27	29 40 29.6	21.32	1.61	21.65	20.98	21.48	21.45	20.49	20.81	21.08	20.89	21.50
	512	104326	...	13 06 30.80	29 30 04.3	21.33	0.21	21.15	20.88	21.06	20.51	20.37	20.22	20.52	20.85	21.20
	1210	110195	...	13 05 10.46	29 39 02.5	21.43	0.24	21.31	20.97	21.33	20.24	19.23	19.36	20.21	20.62	21.02
180.....	670	105643	27	13 05 52.78	29 32 10.4	21.47	0.98	21.26	20.80	21.19	20.90	22.03	21.71	21.42	21.00	21.37
495.....	1935	115180	31	13 06 01.51	29 46 34.2	21.53	0.92	20.62	19.88	20.64	20.38	20.09	20.10	20.61	20.06	20.41
153.....	575	104855	67	13 06 57.73	29 30 55.4	21.55	1.30	22.37	21.33	22.34	22.12	...	21.33	21.52	20.69	21.64
627.....	2325	118122	63	13 06 47.33	29 51 21.6	21.56	0.68	21.41	20.65	21.45	21.33	21.89	21.66	21.93	21.21	22.10
683.....	2494	119387	51	13 06 28.60	29 53 56.0	21.86	1.46	22.09	21.18	22.08	22.06	21.99	21.13	21.62	20.68	21.73
114.....	432	103707	70	13 07 04.00	29 29 03.2	21.88	0.94	21.99	21.11	21.80	21.93	21.48	21.51	21.70	20.75	21.62
152.....	574	104882	23	13 05 49.22	29 30 57.1	21.92	1.47	21.54	21.15	21.44	21.11	20.71	20.39	21.17	21.16	21.38
91	334	102888	68	13 07 03.68	29 27 43.9	21.96	1.33	21.80	20.69	21.51	21.36	21.19	21.51	21.27	20.79	21.74
274.....	970	108169	...	13 05 38.70	29 36 07.4	22.04	0.74	21.89	21.74	21.93	21.60	21.13	21.27	21.60	21.55	21.72
44	136	101392	35	13 06 07.48	29 24 41.5	22.16	3.08	22.17	23.38	22.05	21.56	21.86	21.47	21.63	22.93	22.10
261.....	931	107822	9	13 05 19.62	29 35 34.9	22.17	2.46	21.58	21.03	21.58	21.46	22.63	22.73	21.73	21.05	21.55
384.....	1400	111450	36	13 06 07.54	29 40 59.5	22.22	0.96	21.88	21.56	21.96	22.13	23.47	22.82	22.17	21.73	22.02
329.....	1172	109877	30	13 06 00.43	29 38 32.0	22.25	2.12	22.13	21.51	21.97	21.72	20.74	20.56	21.60	21.22	21.71
445.....	1696	113412	58	13 06 43.56	29 43 45.1	22.26	2.08	22.06	21.35	22.13	22.34	23.36	22.78	22.15	21.30	22.09
	635	105334	...	13 07 21.35	29 31 44.0	22.36	0.30	22.21	21.61	22.06	21.79	20.69	21.48	21.53	21.77	22.26
208.....	744	106442	56	13 06 41.93	29 33 26.8	22.39	2.12	21.19	20.53	21.23	21.28	21.36	21.16	21.08	20.47	21.07
333.....	1178	109934	16	13 05 43.25	29 38 36.9	22.43	2.53	21.03	20.95	21.11	21.25	20.87	21.33	21.56	21.20	21.42
338.....	1189	110028	1	13 04 49.59	29 38 45.8	22.51	0.65	22.35	21.49	22.44	22.22	22.02	21.00	22.25	21.43	22.20

NOTE.—Units of right ascension are hours, minutes, and seconds, and units of declination are degrees, arcminutes, and arcseconds. N_{694} is the serial number of pointlike objects in T89, N_{2540} refers to the catalog described in BTK98, N_{ser} is the serial number of the matching objects in the catalog of Koo 1986 as reported by Munn et al. 1997, and KKC86 is the serial number in Koo et al. 1986. The magnitude m_4 in col. (7) is computed in a circular aperture of 1.″1 on the B_J plate MPF 1053 as in T89. The redshifts z are taken from T89 and T94. Cols. (9)–(17) contain the magnitudes in the same aperture of 1.″1 of m_4 obtained from the indicated plates. Table 2 is also available in machine-readable form in the electronic edition of the Astrophysical Journal.

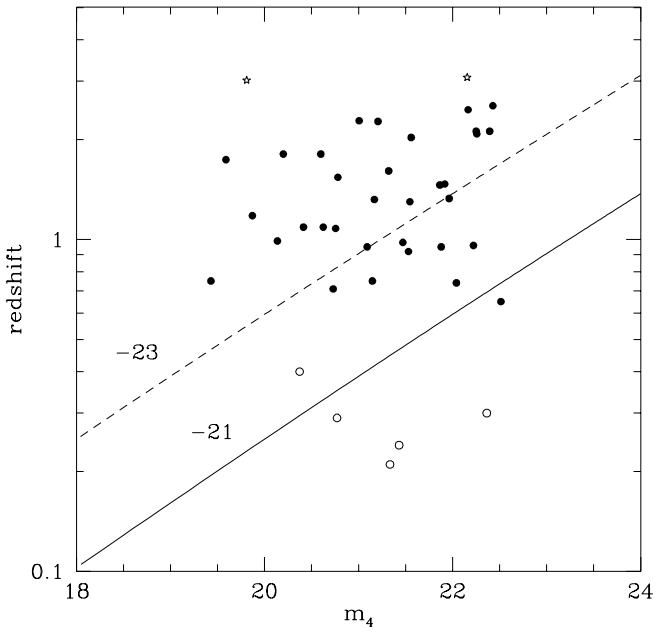

FIG. 1.—Redshift of all the objects of the sample vs. the apparent magnitude (m_4), defined as the B_J magnitude evaluated in a fixed aperture of radius of 1.″1. The stars represent the two highest redshift objects. The open circles represent the five objects with extended images from BTK98. Lines of constant luminosity $M_J = -23$ and $M_J = -21$ are drawn assuming $H_0 = 50\ \mathrm{km\ s^{-1}\ Mpc^{-1}}$, $q_0 = 0.5$, and $\alpha = -1$.

110195 with $z = 0.243$ and N_{ser} 114264 with $z = 0.287$, belong to the sample of BTK98 and are relatively faint AGNs, with $M_{B_J} = -19.6$ and $M_{B_J} = -20.7$, respectively. Their rms variability is among the lowest in the sample of BTK98. Since we know that, in general, fainter AGNs show a stronger variability, we may argue that in this case the light from the nucleus is diluted by the stellar light of the host galaxy. This could also explain the steep spectrum. If so, the spectral changes would also be affected by the presence of a constant stellar component. Two other steep-spectrum objects are the most distant in the sample, N_{ser} 111610 with $z = 3.02$ and N_{ser} 101392 with $z = 3.08$, with $M_{B_J} = -20.7$ and $M_{B_J} = -24.9$, respectively (Fig. 2, *bottom right*). Their spectral slopes are strongly affected by intergalactic Lyα absorption. In particular, the B_J band falls in the (rest-frame) region between the emission Lyα and the Lyman limit, and the U band falls beyond the Lyman limit. The relevant fractional attenuation of the continuum can be evaluated as $\gtrsim 0.2$ and $\gtrsim 0.5$, respectively, e.g., from Steidel & Sargent (1987). Notice that, in Figure 2, the downward shift of the F-band flux is due to the normalization at 2000 Å computed from the extrapolation of the steep uncorrected spectrum and is dramatically reduced if the extrapolation to 2000 Å is done after the correction for the Lyα absorption. Once corrected for the absorption, the two spectra become consistent with the average slope $\langle\alpha\rangle \approx -0.5$ of the sample (see Gaillongo, Gratton, & Trèvese 1990). We stress that the changes of the spectral index due to variability are independent of the intergalactic absorption, even though the apparent SED is affected. Figure 3 shows, with arbitrary scale, the data reported in Table 2.

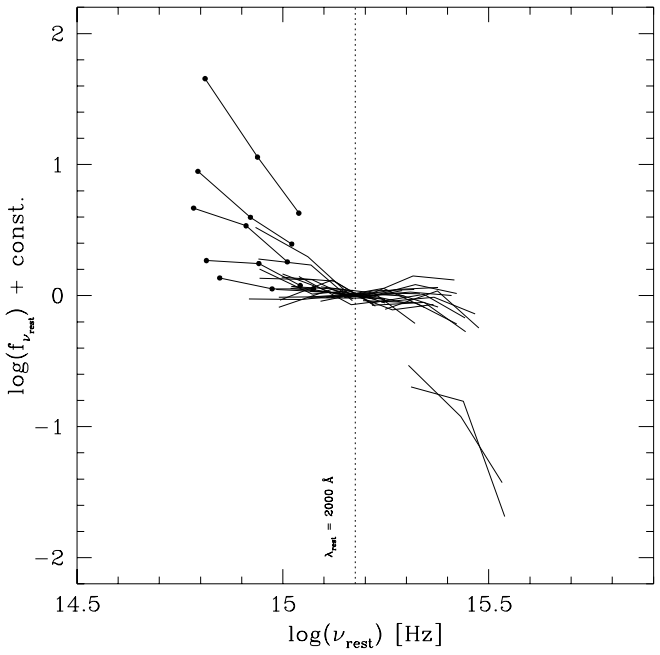

FIG. 2.—U, B_J, and F flux as a function of the rest-frame frequency, normalized at 2000 Å, for the 40 objects of the sample. The photometric data of the five objects from the list of BTK98 are represented by filled circles.

In the majority of the cases the deviations of the SED from a linear $\log f_\nu - \log \nu$ relation are small, but some objects have a local maximum of emission in the observed frequency range. Of course, such a humped SED can be relevant for physical models of the emission mechanism. Correlations of colors with other properties, e.g., the X-ray–optical slope (Miyaji et al. 1997), can be affected by artificial curvature due to nonsimultaneous measures of different bands.

3. VARIABILITY OF THE CONTINUUM SPECTRAL ENERGY DISTRIBUTION

Our aim is to correlate the SED changes with the brightness variations. We do this by correlating the variations $\delta\alpha$ of the spectral slope α, defined by $\log f_\nu \propto \nu^\alpha$, with the variation of $\delta \log f_\nu$, where ν is the rest-frame frequency of one of the observing bands. In order to minimize the effect of noise, we are subject to several restrictions. On average the best signal-to-noise ratio is obtained on J plates; thus, we use pairs of J plates to compute $\delta \log f_{\nu_J}$. The noise in α is lower for larger leverage on the $\log \nu$ axis and the larger the number of bands used. The data used for computing $\delta \log f_{\nu_J}$ must not be used in the calculation of α, otherwise a spurious correlation is found, namely, $\delta\alpha$ and $\delta \log f_{\nu_J}$ appear correlated even in the absence of variability, as a result of the presence of correlated noise in both $\delta\alpha$ and $\delta \log f_{\nu_J}$. This statistical bias may even lead to strong and highly significant correlation (Massaro & Trèvese 1996). It must be considered also that the SED cannot be represented exactly by a power law in the wavelength range studied. This is not a problem as long as α at different epochs is computed in a similar way. In fact, α is a linear combination of the values of $\log f_{\nu_J}$ measured in different bands, thus any deviation of the SED from a power law, while affecting α, does not affect $\delta\alpha$, which is a linear combination of $\delta \log f_{\nu_J}$ values. This is true even when the deviation from the power law is produced by a (nonvariable) absorption in some of the bands. However, computing α in a very different way at two epochs, e.g., using U and N or J and F bands, can generate $\delta\alpha$ values not due to variability. This "spurious"

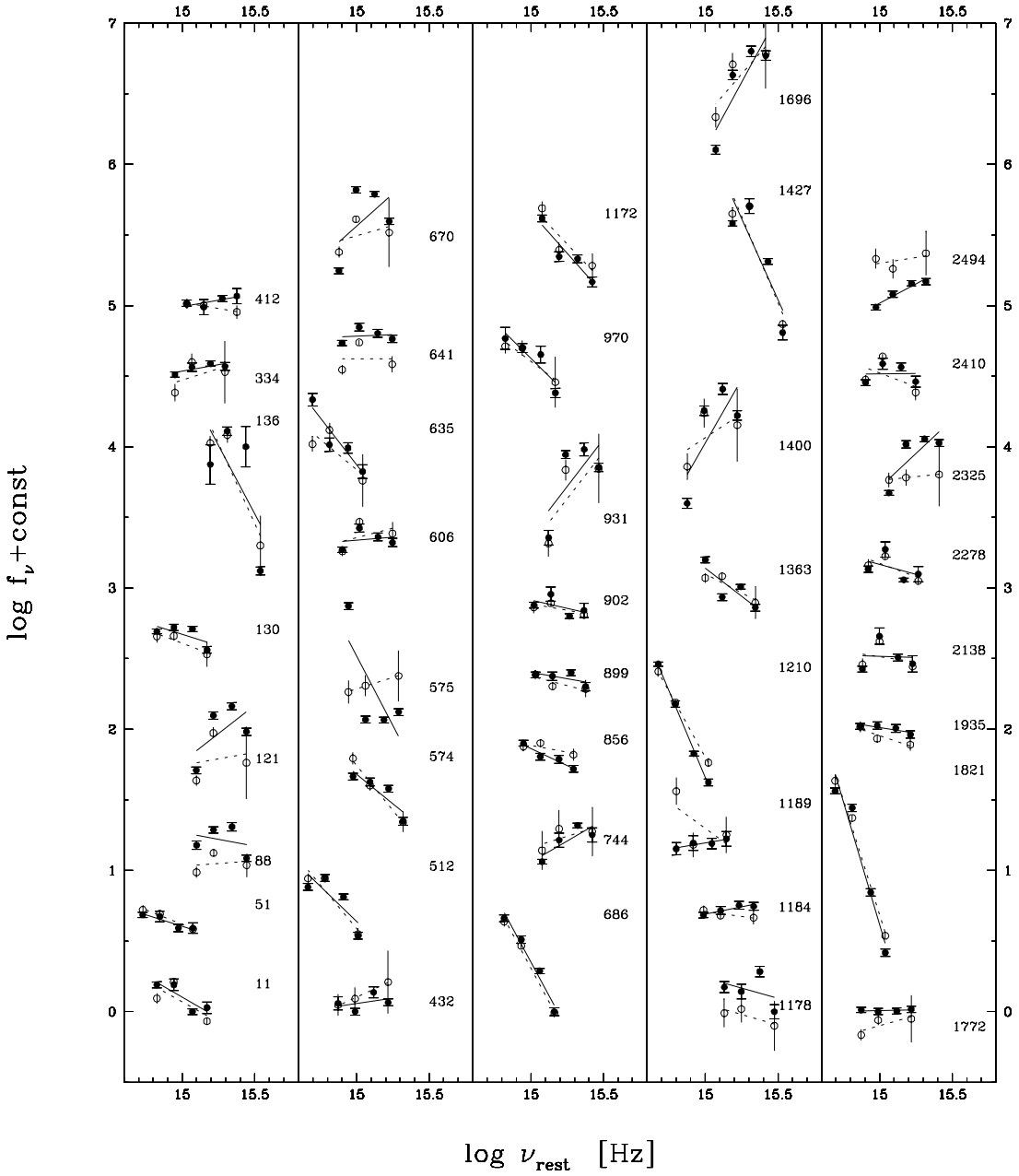

FIG. 3.—Spectral energy distribution in arbitrary scale. *Filled circles*: first epoch; *open circles*: second epoch. The relevant power-law fits are also shown. The scale is the same for each pair of data sets representing the same objects at two different epochs.

$\delta\alpha$ can even be different for two identical QSOs, if they have different redshifts. The above considerations led us to select the two-epoch set of plates described in Table 1, to minimize spurious effects and to increase the reliability and robustness of the results. We determined α from a linear fit in the $\log f_\nu - \log \nu$ plane from U, B_J, F, and N data at the first epoch and from U, F, and N data at the second epoch (the N magnitude of N_{ser} 104855 is missing at the first epoch). In this way two more J plates (MPF 3919 and MPF 3977), one at the first and one at the second epoch, are available to compute an independent $\delta f_{\nu J}$. Emission lines, which are known to vary on the same timescale of the continuum emission, may also affect the spectral slope variations. Whether they cause a positive or negative contribution to the slope depends on the particular band and redshift. Of course, if line variation were perfectly synchronous and proportional to continuum variation, they would not cause any additional slope variability. A recent paper of Kaspi et al. (2000) provides light curves of Hα, Hβ, and Hγ lines and continuum of 28 PG QSOs with a sampling interval of 1–4 months for a total observing period of 7.5 yr. From the line continuum cross-correlation function the authors derive time delays of the order of 100 days for 17 of the 28 QSOs. Hα flux fluctuations are smaller than 20% of the continuum fluctuations. Continuum and line variation are, in general, strongly correlated, and the time width of the cross-correlation function, which depends on the power spectrum of variability, is larger than the delay. As a result, in most cases the cross-correlation at zero time lag is large ($\gtrsim$0.5) so that line variations synchronous and proportion-

al to the continuum variation can be considered a good approximation for the purpose of the present analysis.

Although we cannot correlate the slope changes with flux variations for each individual object, we can study the "ensemble average" of spectral variations of the 40 objects of our sample between two epochs. In Figure 4, $\delta\alpha$ versus $\delta \log f_{\nu_J}$ is reported for the entire sample, with the two linear regression lines, showing an average increase of the spectral slope α for increasing f_J, i.e., a hardening of the spectrum in the brighter phases. The distribution of $\delta\alpha$ values is symmetric about zero, indicating the absence of any strong systematic effect on the spectral slopes. The correlation coefficient between $\delta\alpha$ and $\delta \log f_{\nu_J}$ is $\rho = 0.39$, and the probability of the null hypothesis is $P(>\rho) = 1.28 \times 10^{-2}$. We take the above result as statistical evidence for a relation of the type $\delta\alpha = a + b\,\delta \log f_{\nu_J}$ between α and luminosity variations. To check the dependence of the result on the two most deviant points ($N_{\rm ser} = 118122\,\delta \log f_J = -0.276$ and $N_{\rm ser} = 104885\,\delta \log f_J = 0.292$), we evaluated the correlation excluding in turn (1) both of the points, (2) the first point, and (3) the second point. We obtained, respectively, (1) $\rho = 0.288$, $P(>\rho) = 7.98 \times 10^{-2}$; (2) $\rho = 0.290$, $P(>\rho) = 7.33 \times 10^{-2}$; and (3) $\rho = 0.395$, $P(>\rho) = 1.29 \times 10^{-2}$. To determine the slope b of the above relation, the errors on $\delta\alpha$ and $\delta \log f_{\nu_J}$ must be taken into account, especially if they differ on the two axes. Errors on $\delta \log f_\nu$ for the plate pairs of each band can be computed as follows. From the photometric catalog of the area of sky that has been monitored (KKC86; T89; T94; BTK98), each containing 2540 objects brighter than $B_J = 22.5$, we computed $\delta \log f_{\nu_J}$ for each object and for each band. Then, in each band, we sorted the objects according to their magnitude, and for each object we took the 100 nearest neighbors (in magnitude) and computed the rms value σ_{δ_i} of $\delta \log f_{\nu_i}$ ($i = U, B_J, F, N$), after the exclusion of the points lying more than three standard deviations from the mean. As most of the objects in the field are nonvariable, we assume σ_{δ_i} as a measure of the rms photometric noise on the flux differences δf_{ν_i}. Using the entire plate set, consisting of 5, 15, 5, and 6 plates in the U, B_J, F, and N bands, respectively, it is also possible to derive a magnitude-dependent photometric error for each plate (instead of considering the error on the magnitude difference in plate pairs). As above, we sorted the 2540 objects according to their B_J magnitude (on some reference plate), then for each object we considered the light curve, its time average, and its mean square dispersion, in each band. Then we took 100 neighboring objects in magnitude and computed the rms dispersions around the time average. Neglecting the variance of the time average, this provides an estimate of the rms photometric error of individual plates. The errors estimated from plate pairs are consistent with a quadratic combination of the errors of the relevant individual plates. These errors are shown for each point of Figure 3.

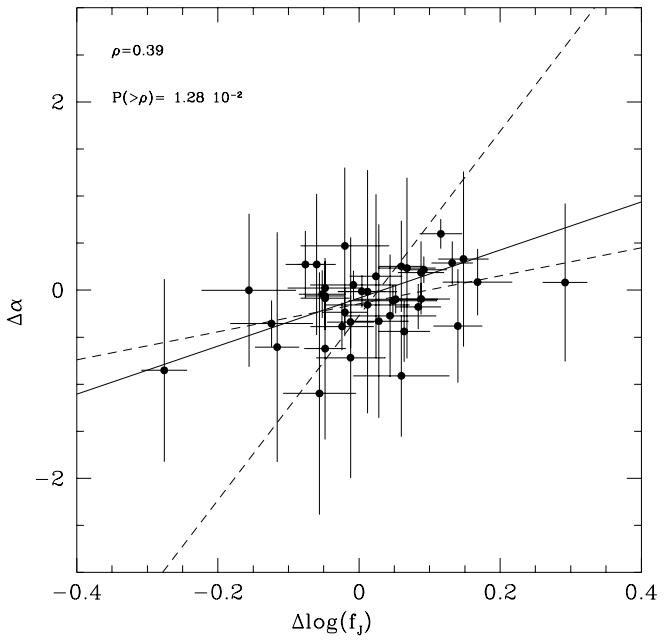

FIG. 4.—Changes of the spectral slope $\delta\alpha$ vs. $\delta \log f_\nu$, with f_ν measured in the B_J band, on independent plates (see text). The dashed lines represent the linear regressions, from which the correlation coefficient ρ is computed. The solid line is the linear fit that takes into account the errors in both coordinates.

The variance of $\delta\alpha$ is a linear combination of the variances of the signals in the bands involved, with appropriate coefficients depending on the frequencies of the bands. We can fit to the $\delta\alpha$ and $\delta \log f_{\nu_J}$ data a straight line taking into account the errors of individual points on both axes. The actual calculation is done using the "fitexy" subroutine from Press & Teukolsky (1992), which gives also the statistical uncertainties on a and b. The result, with 1 σ errors, is $a = (-8.49 \pm 5.50)10^{-2}$ and $b = (2.55 \pm 0.75)$.

Repeating the analysis with the exclusion of the N band reduces the effect of a deviation of the SED from a power law providing a less biased, but more noisy, estimate of the local spectral slope. The correlation is lower but still positive and marginally significant [$\rho = 0.27$, $P(>\rho) = 8.87 \times 10^{-2}$]. The straight-line fit to the data, $a = (-1.67 \pm 3.07)10^{-3}$ and $b = 2.29 \pm 0.37$, is quite consistent with the previous result.

Di Clemente et al. (1996) found that the average increase of variability with redshift is $\Delta S_1/\Delta \log (1 + z) \simeq 0.25$–$0.30$. This quantity is related to the slope b by $\Delta S_1/\Delta \log (1 + z) \simeq \Delta S_1/\Delta \log \nu \simeq \langle \delta\alpha^2 \rangle^{1/2} \simeq b \langle (\delta \log f_\nu)^2 \rangle^{1/2}$, where $\langle \delta\alpha^2 \rangle^{1/2}$ is the rms fluctuation of the spectral slope, S_1 is the variability indicator defined in Di Clemente et al. (1996), and $\langle (\delta \log f_\nu)^2 \rangle^{1/2} \simeq 0.1$ is the rms flux density fluctuation. Thus, the value of b found in the present analysis is consistent with the increase of variability with frequency found by Di Clemente et al. (1996) and confirms the interpretation of the positive v-z correlation suggested by GTV91, by a direct observation of the rms slope variability. We can compare our statistical results with the α– $\log f_\nu$ relation found by Edelson et al. (1990) in individual objects through the analysis of *IUE* observations. All six of their objects have low redshift and are sampled around a wavelength $\lambda \simeq 2000$ Å, which is about the average wavelength of our sample ($\langle z \rangle = 1.365$). For five of their objects they find a significant correlation of α and $\log f_\nu$. For four of these objects the slope b of the relation $\alpha = b \log f_\nu + \text{const}$ is around 1.7, while 3C 273 shows a steeper ($b \approx 2.8$) relation.

It would also be interesting to compare our findings with the variability of $(B-R)$ colors measured by Giveon et al. (1999) in a sample of 42 PG QSOs. Although the average redshift and the rest-frame wavelength region sampled ($\langle z \rangle \simeq 0.12$, $\lambda \approx 3500$ Å) differ from ours, qualitatively their

results agree with ours, namely, they also find a hardening of the spectrum during bright phases. A more detailed and quantitative comparison requires a reanalysis of Giveon et al. (1999) data in a consistent way (D. Trèvese & F. Vagnetti 2001, in preparation; Trèvese & Vagnetti 2000a, 2000b).

4. DISCUSSION AND SUMMARY

Let us assume that the SEDs of the objects of our sample are typical of QSOs, namely, they are dominated by the big blue bump in the spectral region around $\lambda = 2000$ Å (see, e.g., Bregman 1990). We want to check the hypothesis that both the SED slope and brightness changes are caused by temperature changes of an emitting blackbody. For this purpose we use U, B_J, and F data only and we assign the slope α to the intermediate frequency $\log \bar{\nu} = \frac{1}{3} \log (\nu_U \nu_J \nu_F)$. Figure 5 shows α versus $\log \bar{\nu}$ for each object. In the same figure the curves $\alpha(x) \equiv 3 - xe^x/(e^x - 1)$ and $x \equiv h\nu/kT$ of blackbodies are also reported, for various values of the temperature T, h and k being the Planck and Boltzmann constants, respectively.

The two points marked with stars represent the uncorrected SED of the two highest redshift objects, which are affected by the intergalactic Lyα absorption and appear particularly steep. Since SA 57 is close to the Galactic pole, interstellar reddening has a negligible effect on the location of points in Figure 5. The distribution of α is skewed toward negative values, with most objects around -0.5. To check the consistency of slope and brightness variation in a more stringent way, we exclude from the sample the most deviant points, with $\alpha < -2\sigma_\alpha$. Then we obtain $\langle\alpha\rangle = -0.48 \pm 0.68$. The corresponding average temperature is $T \approx 25{,}000$ K. We cannot compare $\delta\alpha/\delta \log f_{\bar{\nu}}$ with α of individual objects because the noise is too large, especially on the former quantity. However, we can compare the slope b of the straight line fitting the points in Figure 4, representing the average increase of the spectral slope α for increasing luminosity, with the corresponding relation expected for blackbody spectra of varying temperature. Brightness and slope variations of the SED of a blackbody of fixed surface are related by $(d\alpha/dT)/(d \log B_\nu/dT) = (\ln 10)[1 - x/(e^x - 1)] \equiv F_{BB}(x)$. In Figure 6, $F_{BB}(x)$ and $\alpha(x)$ are plotted as functions of x. The value of $\langle\alpha\rangle$ and the rms spread σ_α of the sample define an interval of x in this plot. In the same figure are also reported the values of b and $(b - \sigma_b)$ as deduced from the statistical analysis of § 2, which define a lower limit on x.

As seen from Figure 6, the above values define a nonempty region of consistency between $F_{BB}(x)$ and $\alpha(x)$ for the sample. A blackbody with $x \approx 3$ satisfies simultaneously the two constraints. Thus, we can say that the $\delta\alpha$ and $\delta \log f_{\nu_J}$ observed at an average rest frame $\bar{\lambda} \approx 2000$ Å are consistent with temperature variations of a typical blackbody of temperature $T \approx 25{,}000$ K.

A single blackbody spectrum is an oversimplified representation of the SED that, in the case of accretion disks models, ignores temperature gradients and the presence of other components necessary to explain the emission outside the frequency range considered. In any case we can state the following:

1. The increase of the amplitude of variability with the rest-frame frequency (Giallongo et al. 1991; Cristiani et al. 1996; Di Clemente et al. 1996) is due to the hardening in the bright phases (and vice versa) of the spectrum, which to a first approximation maintains its local power-law shape.
2. The rms slope variations are quantitatively consistent with the increase of variability for increasing frequency

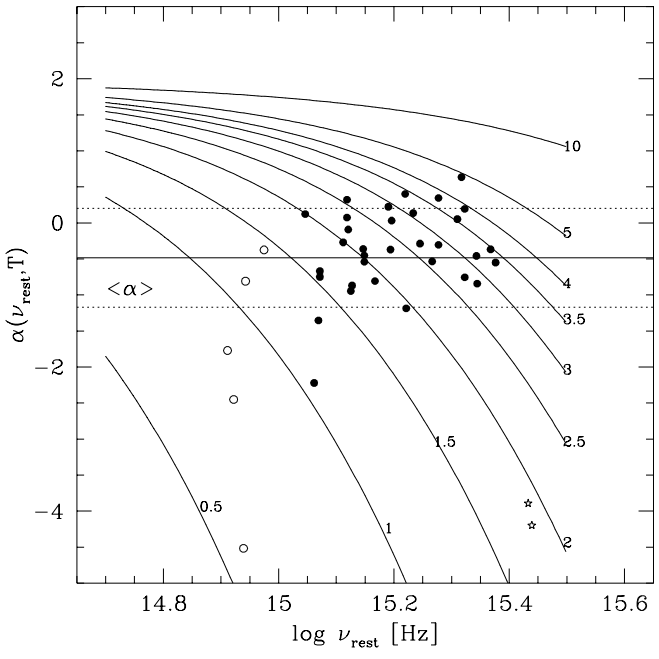

FIG. 5.—Slope α as a function of $x \equiv h\nu/kT$, for the 40 objects of the sample, as computed from U, B_J, and F bands, with $\log \nu = \frac{1}{3} \log (\nu_U \nu_B \nu_F)$. The stars represent the two highest redshift objects whose colors are affected by Lyα absorption. The open circles represent the five objects with extended images from BTK98. The solid lines represent $\alpha(x)$ for blackbodies of different temperatures T, indicated in units of 10^4 K. The horizontal lines represent $\langle\alpha\rangle \pm \sigma_\alpha$, after the exclusion of the three points at more than 2 σ from the mean.

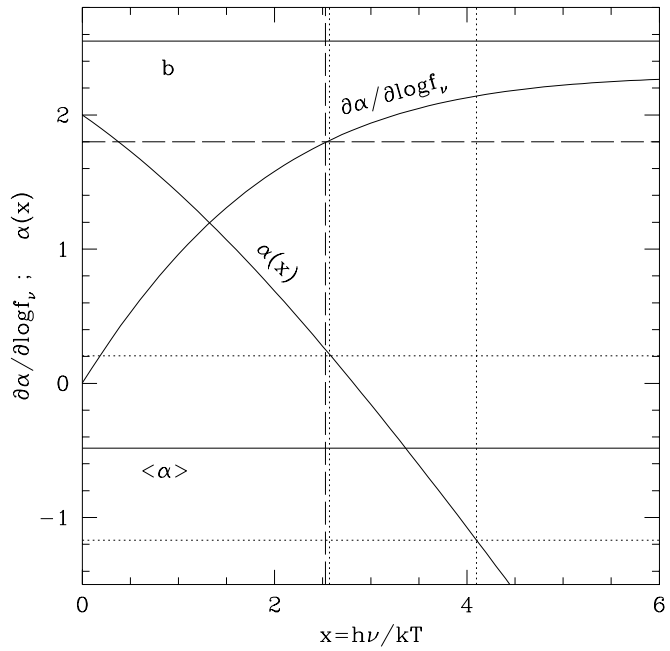

FIG. 6.—Values of $\alpha(x)$ and $F_{BB}(x)$ for a blackbody, as a function of $x \equiv h\nu/kT$. The continuous horizontal lines represent $\langle\alpha\rangle$ and the slope b of the straight line fitting the data in Fig. 3. The dashed and dotted lines represent the 1 σ interval and the relevant bound on x, deriving from the comparison of the data with the blackbody curves $F_{BB}(x)$ and $\alpha(x)$, respectively.

found by Di Clemente et al. (1996). This confirms, by a direct observation of spectral slope changes, that correlation between variability and redshift is accounted for by intrinsic spectral changes and does not require cosmological evolutionary effects.

3. Our results show that the average changes of the SED slope and the relevant flux variations in the optical–UV region are at least not inconsistent with temperature variations of a single emitting blackbody of $T \approx 2.5 \times 10^4$ K.

4. The average relation between slope and brightness variations provides a new constraint on models of the emission mechanism.

For instance, an optically thin plasma model (Barvainis 1993) requires a temperature of the order of 10^6 K to explain with a single emission component the SED from optical–UV to X-ray frequencies (see Fiore et al. 1995). The free-free luminosity $L_\nu \propto T^{-1/2} e^x$ (Rybicki & Lightman 1979) can provide an optical–UV spectral slope α consistent with the observations, but in this case the slope and brightness changes produced by temperature changes are related by $F_{\rm ff}(x) \equiv \partial\alpha/\partial \log f_\nu = x/(x - 1/2)$, i.e. $F_{\rm ff} \simeq -2x$, for $x \ll 1$. Thus, for $T \approx 10^6$, $F_{\rm ff} \approx -0.1$ is not only too small in absolute value, but it is even negative, thus completely inconsistent with the result of our analysis. Notice also that the temperature changes of a simple blackbody of $T \approx 10^5$ K would be inconsistent with our findings since, for $\lambda \approx 2000$ Å, this temperature implies $F_{\rm BB} \simeq 0.27$. In fact, at high temperature any thermal emission approaches the limit where the long-wavelength part has a fixed spectral slope, independent of temperature changes (Paltani & Courvoisier 1994). Any model trying to reproduce the observed SED from the IR to X-rays could be tested against the observed α– $\log f_\nu$ relation. In particular, it is possible to investigate whether the variation of one or some of the parameters involved (like the temperature) is capable of reproducing the observed relation. Perhaps additional phenomena, e.g., hot spots or flares (Krishan & Wiita 1994; Kawaguchi et al. 1998) over an otherwise stationary accretion disk, are needed to explain the SED variability. The main limits of the present analysis are the small amplitude of variability due to the short time interval (1 yr) between the observations and the lack of α– $\log f_\nu$ relation for individual objects, which could be different depending, e.g., on their intrinsic luminosity.

Despite these limits, our results clearly show that a few additional multiband observations, properly distributed in time, could provide strong constraints on the physics of emission and variability, especially if associated with simultaneous observations in the IR and X-rays.

This work was partly supported by the Italian Ministry for University and Research (MURST) under grant Cofin98-02-32.

REFERENCES

Angione, R. J., & Smith, H. J. 1972, in IAU Symp. 44, External Galaxies and Quasi-Stellar Objects, ed. D. S. Evans (New York: Springer), 171
Aretxaga, I., Cid Fernandes, & Terlevich, R. 1997, MNRAS, 286, 271
Aretxaga, I., & Terlevich, R. 1994, MNRAS, 269, 462
Barvainis, R. 1993, ApJ, 412, 513
Bershady, M. A., Trèvese, D., & Kron, R. G. 1998, ApJ, 496, 103 (BTK98)
Bregman, J. N. 1990, A&A Rev., 2, 125
Cristiani, S., Trentini, S., La Franca, F., Aretxaga, I., Andreani, P., Vio, R., & Gemmo, A. 1996, A&A, 306, 395
Cristiani, S., Vio, R., & Andreani, P. 1990, AJ, 100, 56
Cutri, R. M., Wisniewski, W. Z., Rieke, G. H., & Lebofski, H. J. 1985, ApJ, 296, 423
Di Clemente, A., Natali, G., Giallongo, E., Trèvese, D., & Vagnetti, F. 1996, ApJ, 463, 466
Edelson, R. 1992, ApJ, 401, 516
Edelson, R. A., Krolik, J. H., & Pike, G. F. 1990, ApJ, 359, 86
Fiore, F., Elvis, M., Siemiginowska, A., Wilkes, B. J., McDowell, J. C., & Mathur, S. 1995, ApJ, 449, 74
Giallongo, E., Gratton, R., & Trèvese, D. 1990, MNRAS, 244, 450
Giallongo, E., Trèvese, D., & Vagnetti, F. 1991, ApJ, 377, 345 (GTV91)
Giveon, U., Maoz, D., Kaspi, S., Netzer, H., & Smith, P. S. 1999, MNRAS, 306, 637
Green, A. R., McHardy, I. M., & Letho, H. J. 1993, MNRAS, 265, 664
Hawkins, M. R. S. 1983, MNRAS, 202, 571
———. 2000, A&AS, 143, 465
Hawkins, M. R. S., & Véron, P. 1993, MNRAS, 260, 202
———. 1996, MNRAS, 281, 348
Hook, I. M., McMahon, R. G., Boyle, B. J., & Irwin, M. J. 1994, MNRAS, 268, 305
Kaspi, S., Smith, P. S., Netzer, H., Maoz, D., Jannuzi, B. T., & Giveon, U. 2000, ApJ, 533, 631
Kawaguchi, T., Mineshige, S., Umemura, M., & Turner, E. L. 1998, ApJ, 504, 671
Kinney, A. L., Bohlin, R. C., Blades, J. C., & York, D. G. 1991, ApJS, 75, 645
Koo, D. C. 1986, ApJ, 311, 651
Koo, D. C., & Kron, R. G. 1988, ApJ, 325, 92
Koo, D. C., Kron, R. G., & Cudworth, K. M. 1986, PASP, 98, 285 (KKC86)
Krishan, V., & Wiita, P. J. 1994, ApJ, 423, 172
Kron, R. G., & Chiu, L.-T. 1981, PASP, 93, 397
Majewski, S. R., Munn, J. A., Kron, R. G., Bershady, M. A., Smetanka, J. J., & Koo, D. C. 1991, in ASP Conf. Proc. 21, The Space Distribution of Quasars, ed. D. Crampton (San Francisco: ASP), 55
Massaro, E., et al. 1996, A&A, 314, 87
Massaro, E., & Trèvese, D. 1996, A&A, 312, 810
Miyaji, T., Connoly, A. J., Szalay, A. S., & Boldt, E. 1997, A&A, 323, L37
Munn, J. A., Koo, D. C., Kron, R. G., Majewski, S. R., Bershady, M. A., & Smetanka, J. J. 1997, ApJS, 109, 45
Mushotzki, R. F., Done, C., & Pounds, K. A. 1993, ARA&A, 31, 717
Paltani, S., & Courvoisier, T. J.-L. 1994, A&A, 291, 74
Pica, A. J., & Smith, A. G. 1983, ApJ, 272, 11
Press, W. H., & Teukolsky, S. A. 1992, Comput. Phys., 6, 274
Rees, M. 1984, ARA&A, 22, 741
Rybicki, G. B., & Lightman, A. P. 1979, Radiative Processes in Astrophysics (New York: Wiley)
Steidel, C. C., & Sargent, W. L. W. 1987, ApJ, 313, 171
Trèvese, D., Kron, R. G., Majewski, S. R., Bershady, M. A., & Koo, D. C. 1994, ApJ, 433, 494 (T94)
Trèvese, D., Pittella, G., Kron, R. G., Koo, D. C., & Bershady, M. A. 1989, AJ, 98, 108 (T89)
Trèvese, D., & Vagnetti, F. 2000a, Proc. Guillermo Haro Advanced Lectures on the Starburst-AGN Connection (Tonantzintla, Mexico, 2000 June 26–30), in press (astro-ph/0011076)
———. 2000b, Proc. 4th Italian Meeting on AGN, AGN nel 2000 (Trieste, 2000 May 15–18), in press (astro-ph/0007161)
Ulrich, M. H., Maraschi, L., & Urry, C. M. 1997, ARA&A, 35, 445
Uomoto, A. K., Wills, B. J., & Wills, D. 1976, AJ, 81, 905